The SSDC Role in the LICIACube Mission: Data Management and the MATISSE Tool

Angelo Zinzi[1,2], Vincenzo Della Corte[3], Stavro L. Ivanovski[4], Alice Lucchetti[5], Elena Mazzotta Epifani[6], Federico Miglioretti[7], Maurizio Pajola[5], Alessandro Rossi[8], Olivier Barnouin[9], Raymond C. Espiritu[9], Elisabetta Dotto[6], Marilena Amoroso[1], Ivano Bertini[3,10], John R. Brucato[11], Andrea Capannolo[12], Gabriele Cremonese[5], Biagio Cotugno[7], Massimo Dall'Ora[13], Jasinghege D. P. Deshapriya[6], Valerio Di Tana[7], Igor Gai[14], Pedro H. A. Hasselmann[6], Simone Ieva[6], Gabriele Impresario[1], Michèle Lavagna[12], Andrea Meneghin[11], Dario Modenini[14,15], Davide Perna[6], Simone Pirrotta[1], Giovanni Poggiali[11], Pasquale Palumbo[3,10], Emanuele Simioni[5], Simone Simonetti[7], Paolo Tortora[14,15], Marco Zannoni[14,15], and Giovanni Zanotti[12]

[1] Agenzia Spaziale Italiana, Via del Politecnico, snc, I-00133, Roma, Italy; angelo.zinzi@ssdc.asi.it
[2] Space Science Data Center—ASI, Via del Politecnico, snc, I-00133, Roma, Italy
[3] INAF Istituto di Astrofisica e Planetologia Spaziali, Via Fosso del Cavaliere 100, I-00133, Roma, Italy
[4] INAF Osservatorio Astronomico di Trieste, Via G.B. Tiepolo, 11, I-34143, Trieste, Italy
[5] INAF Osservatorio Astronomico di Padova, Vicolo Osservatorio, 5, I-35122, Padova, Italy
[6] INAF Osservatorio Astronomico di Roma, Via Frascati 33, I-00078, Monte Porzio Catone, Roma, Italy
[7] Argotec, Via Cervino, 52, I-10155, Torino, Italy
[8] CNR Istituto di Fisica Applicata "Nello Carrara", Via Madonna del Piano 10, I-50019, Sesto Fiorentino, Firenze, Italy
[9] The Johns Hopkins University Applied Physics Laboratory, Laurel, MD, USA
[10] Università degli Studi di Napoli "Parthenope", Dipartimento di Scienze & Tecnologie, Centro Direzionale, Isola C4, I-80143, Napoli, Italy
[11] INAF Osservatorio Astrofisico di Arcetri, Largo Enrico Fermi 5, I-50125, Firenze, Italy
[12] Politecnico di Milano - Bovisa Campus, Dipartimento di Scienze e Tecnologie Aerospaziali, Via La Masa 34, I-20156, Milano, Italy
[13] INAF Osservatorio Astronomico di Capodimonte, Salita Moiariello, 16, I-80131, Napoli, Italy
[14] Alma Mater Studiorum - Università di Bologna, Dipartimento di Ingegneria Industriale, Viale Fontanelle 40, I-47121, Forlì, Italy
[15] Alma Mater Studiorum - Università di Bologna, Centro Interdipartimentale di Ricerca Industriale Aerospaziale, Via B. Carnaccini 12, I-47121, Forlì, Italy

Abstract

Light Italian Cubesat for Imaging of Asteroids (LICIACube) is an Italian mission managed by the Italian Space Agency (ASI) and part of the NASA Double Asteroid Redirection Test (DART) planetary defense mission. Its main goals are to document the effects of the DART impact on Dimorphos, the secondary member of the (65803) Didymos binary asteroid system, characterizing the shape of the target body and performing dedicated scientific investigations on it. Within this framework, the mission Science Operations Center will be managed by the Space Science Data Center (ASI-SSDC), which will have the responsibility of processing, archiving, and disseminating the data acquired by the two LICIACube onboard cameras. In order to better accomplish this task, SSDC also plans to use and modify its scientific webtool Multi-purpose Advanced Tool for Instruments for the solar system Exploration (MATISSE), making it the primary tool for the LICIACube data analysis, thanks to its advanced capabilities for searching and visualizing data, particularly useful for the irregular shapes common to several small bodies.

Unified Astronomy Thesaurus concepts: Asteroids (72)

1. Introduction

Launched on 2021 November 24, the NASA Double Asteroid Redirection Test (DART) will be the first mission able to demonstrate the applicability of the kinetic impactor method for planetary defense (Cheng et al. 2018). The main spacecraft, with a mass of 650 kg, aims at impacting Dimorphos (on 2022 September 26), the secondary member of the (65803) Didymos binary asteroid system, at an estimated speed of about 6.6 km s^{-1}.

This mission carries the 6U cubesat Italian Space Agency (ASI) Light Italian Cubesat for Imaging of Asteroids (LICIACube; Dotto et al. 2021), manufactured by Argotec, as a piggyback, which will be released about 10 days before the DART impact, performing an autonomous flyby of the target and witnessing the impact by means of its two different cameras, LICIACube Explorer Imaging for Asteroid (LEIA) and LICIACube Unit Key Explorer (LUKE).

Up to now, the scientific mission is expected to last for some minutes around the closest approach (expected at a distance from the target of roughly 50 km), even if the data downlink, due to the low available data rate, will last for some months.

LEIA is a panchromatic narrow-field camera expected to provide high-resolution (i.e., up to 1.38 m pixel^{-1}) images of the impact site (Pajola et al. 2022, this focus issue), as well as contributing to a better definition of the target body shape with the acquisition of images coming from the Dimorphos hemisphere not observed by DRACO, the camera installed on board DART.

LUKE is an RGB wide-field camera (Poggiali et al. 2022, this focus issue) whose characteristics should allow for performing dedicated scientific observations, such as the study of the color variations over the Dimorphos surface.

After being received at the Argotec Mission Control Center (MCC) from the Deep Space Network (DSN), all of the data acquired by LICIACube will be stored, processed, archived, and distributed at the LICIACube Science Operations Center (SOC), coordinated by the ASI Space Science Data Center (SSDC).

In this work, we will describe the processes behind the data management at the LICIACube SOC, first by highlighting the SSDC's long-lasting experience in space data management (Section 2), then by depicting the actual procedures designed to make the data ready for science (Section 3) and available to the community thanks to the SSDC Multi-purpose Advanced Tool for Instruments for the solar system Exploration (MATISSE) scientific webtool (Section 4).

An outline of how the LICIACube mission objectives could benefit all of these processes will be given in Section 5.

2. SSDC Heritage in Space Data Management and Exploitation

The ASI-SSDC was established in 2000 as a multimission facility linked to high-energy astrophysics data management and exploitation and named the ASI Science Data Center (ASDC). The ASDC was an evolution of the data center of the BeppoSax X-ray astronomy satellite, which started its activities in the early 1990s. After this long-lasting initial phase, predominantly dedicated to high-energy astrophysics missions, in the last decade, the center has begun to increasingly include different branches of space science, such as stellar physics and planetary and exoplanetary sciences.

The SSDC is mainly focused on the archiving, analysis, and distribution of space mission data and the development of scientific tools, thus allowing one to extract high-level scientific information from the archived data sets. Such a goal is achieved through a characteristic "operative approach" involving both scientists and industrial partners.

As a consequence of this approach, the center is constituted of personnel from the ASI, the National Institute for Astrophysics (Istituto Nazionale di Astrofisica, INAF), and the National Institute for Nuclear Physics (Istituto Nazionale di Fisica Nucleare), with information and communication technology support provided by industrial partners (currently Telespazio and Serco). It is hence possible to follow the real needs of the scientific community of reference, as demonstrated by "cornerstone" tools such as the Multi Mission Interactive Archive, the Spectral Energy Distribution Tool, and MATISSE.

2.1. SSDC for the Planetary Sciences

The expansion of SSDC activities to solar system exploration missions has been characterized by the development of MATISSE, whose first release dates back to 2013 (Zinzi et al. 2016) and is now available in version 2.0 (https://tools.ssdc. asi.it/Matisse; Zinzi et al. 2021).

Because one of the main MATISSE capabilities is the possibility of projecting and viewing the data on the 3D shape model of the target directly in a web browser, its application to data acquired by missions devoted to small bodies has been straightforward (e.g., Longobardo et al. 2018; Zinzi et al. 2018). An example of the MATISSE capabilities is given in Figure 1.

In particular, the contribution of MATISSE has been essential for the ESA Rosetta mission to the comet 67P Churyumov–Gerasimenko, helping the scientific team to overcome the difficulties related to the very irregular shape of the comet nucleus and achieve some major scientific outcomes (e.g., Ciarniello et al. 2016; Quirico et al. 2016; Longobardo et al. 2017; Tosi et al. 2019).

In addition to the possible fruitful exploitation of LICIA-Cube data with MATISSE, other SSDC activities can be easily linked to the LICIACube mission. Indeed, in recent years, the center has been involved in a series of projects for the study of near-Earth objects (NEOs), such as NEOROCKS (Dotto et al. 2021; Zinzi et al. 2021). Once integrated, these projects can be part of a well-established program, where all data of potential interest for the scientific exploitation of NEOs (which Didymos belongs to) could be easily accessed and rapidly analyzed by means of the SSDC dedicated infrastructure.

These efforts could be considered as the starting seed of a future ASI NEO Center able to exploit the SSDC infrastructure and expertise in the wider framework of the new Space Program of the European Union.

3. LICIACube SOC Activities at SSDC

The main goals of the LICIACube SOC are to process, archive, and disseminate the data acquired by LEIA and LUKE.

In order to fulfill these tasks, a well-defined architecture has been designed, starting from the LICIACube spacecraft, passing through the DSN and the LICIACube MCC (where the output of the navigation team by University of Bologna is stored), located on the Argotec premises, and with a strict collaboration between ASI-SSDC and INAF.

The designed and expected data flow is depicted in Figure 2, and the SOC role in this process begins with the conversion to the FITS format standardized to be compliant with the PDS4 requirements of the raw-from-telemetry images received by the MCC.

It is worth noting that the LICIACube SOC only has two connections inside the ground segment design depicted in Figure 2: the one with the LICIACube MCC and the one with the DART SOC.

This is because the main aim of the LICIACube SOC is related to the dissemination of science-ready data. Therefore, it retrieves raw-from-telemetry images, together with the relevant metadata, from the MCC (links 8 and 9 in Figure 2) and, after the conversion to standardized FITS images, makes them available to the rest of the DART/LICIACube teams (link 5 in Figure 2).

We underline that this step does not change the bit depth of the images, which remains at 16 bits pixel^{-1} for LEIA and 8 bits pixel^{-1} for LUKE, or the image data content. However, the FITS file, different from the raw-from-telemetry file sent by the MCC, contains a set of metadata as FITS keywords, useful to better constrain and archive the image data (see Tables 1 and 2).

A more robust image processing is performed for the calibration procedure. In this case, following the conversion of the image from digital number (DN) to physical units (i.e., radiance), the image is formatted at 32 bits pixel^{-1} instead of the 16 or 8 (for LEIA and LUKE, respectively) used for the raw one, and additional FITS keywords are added (see Tables 3 and 4) with respect to the raw FITS in order to accurately map the calibration process.

Albeit the calibration procedure is still not completely fixed, what is currently expected is that the calibration FITS files for LEIA are formatted as $7 \times 2048 \times 2048$ (for LUKE, $7 \times 2048 \times 1088$) with the following planes.

1. Plane 0: bias for corresponding (I, j) pixel in DN.
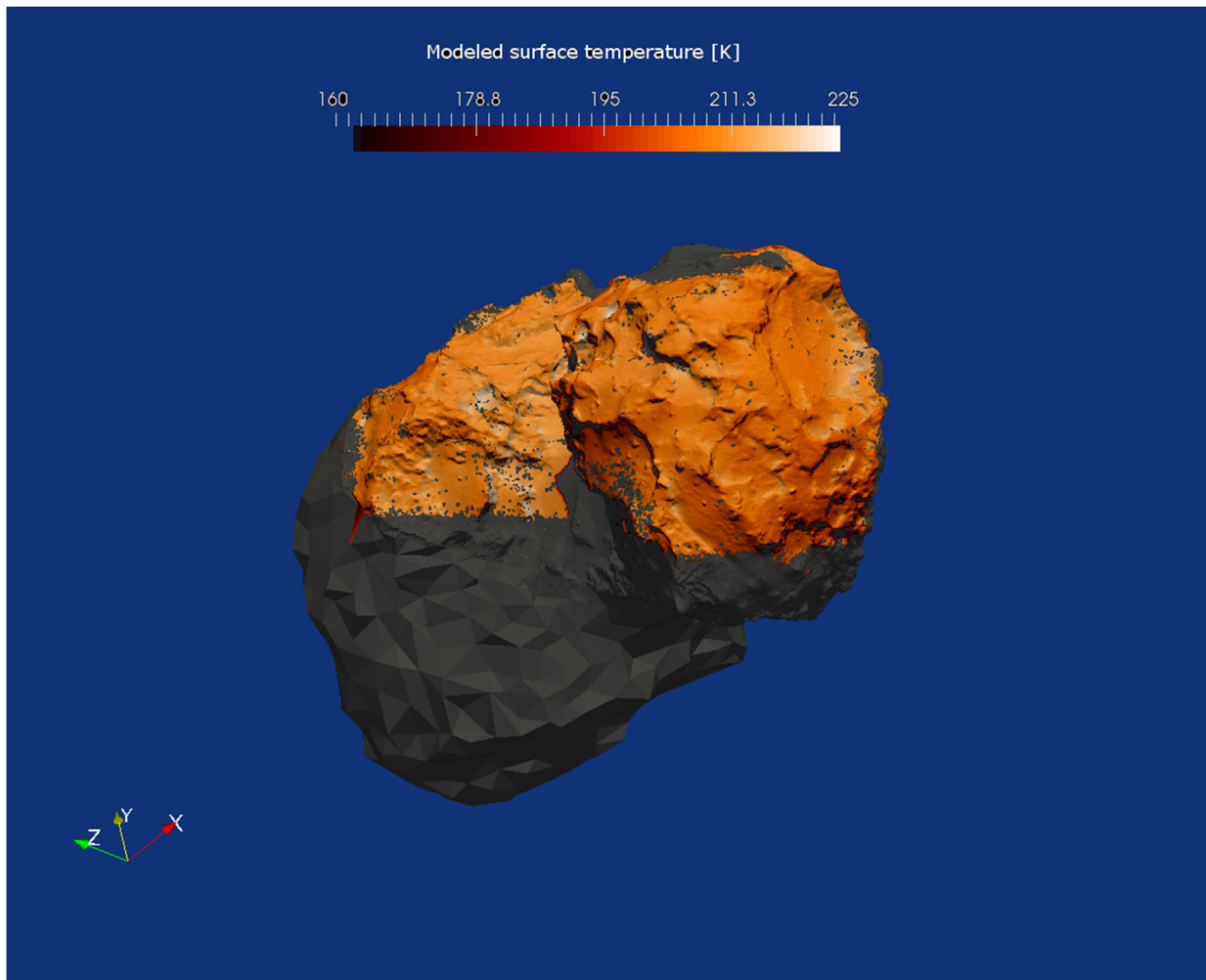
Figure 1. Surface data (i.e., modeled temperature) projected over the 67P comet nucleus shape model as visualized by MATISSE. This image has been generated using observations and models not available to the public and described by Tosi et al. (2019), where more details about it can be found.
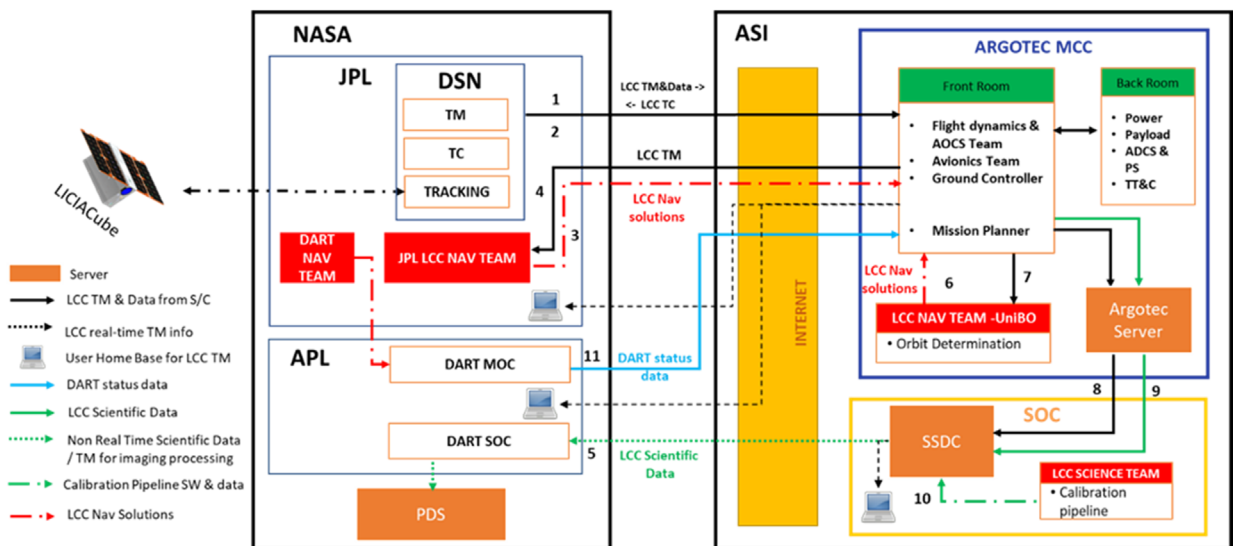
Figure 2. Data flow and communication of the LICIACube Mission and SOC. Acronyms are as follows: Applied Physics Laboratory (APL), Jet Propulsion Laboratory (JPL), Deep Space Network (DSN), Telemetry (TM), Telecommands (TC), Navigation (NAV), LICIACube (LCC), Attitude and Orbital Control System (AOCS), Attitude Determination & Control Subsystem (ADCS), Propulsion Subsystem (PS), and Telemetry Tracking & Command (TT&C).

Table 1
FITS Metadata for the LEIA Raw Images

Keyword and Example	Description
SIMPLE = T/file conforms to FITS standard	Required in FITS standard
BITPIX = 16/number of bits per data pixel	LEIA raw images delivered to the SOC will always be 16 bit. Calibrated images are the result of applying the calibration files, themselves in 32 bit floating point, to the raw images. All are stored in big endian as per the FITS standard.
NAXIS = 2/number of data axes	Number of data axes; all LEIA images have two axes
NAXIS1 = 2048/length of data axis 1	Number of rows
NAXIS2 = 2048/length of data axis 2	Number of columns
WINXSTA = "−1"/X origin of window	Column where window starts. Window coordinates are with respect to a 2048 × 2048 image. The upper left-hand corner of the image plus header row is coordinate 0, 0. −1 if second windowing not applied.
WINYSTA = "−1"/Y origin of window	Row where window starts. Window coordinates are with respect to a 2048 × 2048 image. The upper left-hand corner of the image plus header row is coordinate 0, 0. −1 if second windowing not applied.
WINXEND = "2048"/X end of window	Column where window ends. Window coordinates are with respect to a 2048 × 2048 image. The upper left-hand corner of the image plus header row is coordinate 0, 0. −1 if second windowing not applied.
WINYEND = "2048"/X end of window	Row where window ends. Window coordinates are with respect to a 2048 × 2048 image. The upper left-hand corner of the image plus header row is coordinate 0, 0. −1 if second windowing not applied.
EXTEND = T/FITS data set may contain extensions	By default, set to T so that we can add extensions if needed
DATE = "2018-08-25T09:23:89"/FITS header creation date YYYY-MM-DDTHH:MM:SS	Time fits file was created by the SOC; for calibrated and derived, it is the creation time of the product
MISSION = "DART"/mission: DART	Name of mission
HOSTNAME = "LICIACube"/spacecraft name	LEIA is on the spacecraft named LICIACube
INSTRUME = "LEIA"/instrument name	Instrument name
APID	Application ID of science image data: the images themselves
TARGET = "DIDYMOS"/target object	Primary target object
MPHASE = "TERMINAL"/phase of the mission	The DART mission is divided into phases; this keyword states the phase during which the image was acquired.
IMG_TIME = "298271898.013220"/[s] image TOV	Start of image capture time in spacecraft clock notation. The number preceding the decimal point is integer seconds. The number after the decimal point is subsecond clock ticks, where each tick represents TBD microseconds.
IMG_UTC = "2022 OCT 01 10:28:09.600"/image TOV in UTC	Start of image capture time in UTC
SCLKNAME = "liciacube_sclk_0000.tsc"/SCLK file used for IMG_UTC	Name of SCLK file used to compute IMG_UTC
READOUT = "87.46666"/readout time in microseconds	Global readout time
EXPTIME = "0.156789"/[s] exposure time	Image exposure time in seconds
GAIN = 1 /gain setting	Detector gain setting
BINNING = "ON"/binning status	If binning is on or not
TRUNC = "MSB"/truncation mode	Defines whether the data are truncated using MSB or LSB. When binning is enabled, the truncation mode is MSB. When binning is disabled, the truncation mode is LSB.
RCNTTHST = 1/thruster firing flag	Flag for whether thrusters were fired within one settling time before this image; 1 = true, 0 = false (TBR)
AOCWX = 0/[deg s^{-1}] rotation speed on X-axis	Rotation speed of LICIACube frame X-axis
AOCWY = 0/[deg s^{-1}] rotation speed on Y-axis	Rotation speed of LICIACube frame Y-axis

Table 1
(Continued)

Keyword and Example	Description
AOCWY = 0/[deg s^{-1}] rotation speed on Z-axis	Rotation speed of LICIACube frame Z-axis
DETTEMP = 18.333/[degC] detector temperature	LEIA detector temperature
EPHMETA = "LCC210701-EMK-RN-L211124-V001.mk"/ephemeris meta-kernel to be used	Ephemeris metakernel to be used
ATTMETA = "LCC201228-AMK-RN-L221124-V001.mk"/attitude metakernel to be used	Attitude metakernel to be used
CORT_UTC	UTC time at mid-exposure time (=IMGTIME+0.5EXPTIME) used to define attitude and representative observing geometry
CORTJDAT	Julian Ephemeris Date based at mid-exposure (=IMGTIME+0.5EXPTIME) used to define attitude and representative observing geometry
SOCQUATA = "0.10808003767484" /SC quaternion in J2000 (q0) using A CORT_UTC	Spacecraft quaternion computed by the SOC using SPICE and CORT_UTC
SOCQUATX = "−0.674302095900066" /SC quaternion in J2000 (q1) using CORT_UTC	
SOCQUATY = "−0.32453616895850" /SC quaternion in J2000 (q2) using CORT_UTC	
SOCQUATZ = "0.65445524213556" /SC quaternion in J2000 (q3) using appropriate CORT_UTC time	
BORE_RA = "326.459994"/[deg] boresight R.A.	Boresight R.A.
BORE_DEC = "−38.093559"/[deg] boresight decl.	Boresight decl.
CELN_CLK = "28.16" /[deg] celestial north clock angle	Celestial north clock angle
ECLN_CLK = "49.30" /[deg] ecliptic north clock angle	Ecliptic north clock angle
SUN_CLK = "318.40"/[deg] Sun clock angle	Sunward direction clock angle
PXARCS = "1.02"/[arcsec] pixel scale	Pixel scale in arcseconds
PXMRAD = "4.96"/[microradians] pixel scale	Instantaneous field of view of a pixel in microradians. If BINNING = ON, this value is reported for a 2 × 2 binned pixel.
PHDIST = "1.04"/[au] heliocentric distance—primary	Distance between the Sun and the primary target in au
PSCRNG = "4.2622E+02"/[km] spacecraft range—primary	Distance between the spacecraft and the primary target center in kilometers
PSPHASE = "55.98"/[deg] solar phase angle—primary	Angle between the sunward direction and the direction to the spacecraft as observed from the primary target
PSELON = "73.49"/[deg] solar elongation—primary	Angle between the sunward direction and the direction to the primary target as observed from the spacecraft
PPPCLK = "228.64"/[deg] positive pole clock angle—primary	Positive pole clock angle of the primary target
PSUBLAT = "38.04"/[deg] subobserver latitude—primary	Subobserver latitude of the primary target
PSUBLON = "146.65"/[deg] subobserver longitude—primary	Subobserver east longitude of the primary target
PSSOLLAT = "−1.07"/[deg] subsolar latitude—primary	Subsolar latitude of the primary target
PSSOLLON = "190.18"/[deg] subsolar longitude—primary	Subsolar east longitude of the primary target
SHDIST = "1.04"/[au] heliocentric distance—secondary	Distance between the Sun and the secondary target in au
SSCRNG = "4.2623E+02"/[km] spacecraft range—secondary	Distance between the spacecraft and the secondary target center in kilometers
SSPHASE = "56.14"/[deg] solar phase angle—secondary	Angle between the sunward direction and the direction to the spacecraft as seen from the secondary target
SSELON = "73.59"/[deg] solar elongation—secondary	Angle between the sunward direction and the direction to the secondary target as observed from the spacecraft
SPPCLK = "228.64"/[deg] positive pole clock angle—secondary	Positive pole clock angle of the secondary target

<div align="center">**Table 1**</div>
<div align="center">(Continued)</div>

Keyword and Example	Description
SSUBLAT = "38.09"/[deg] subobserver latitude—secondary	Subobserver latitude of the secondary target
SSUBLON = "146.46"/[deg] subobserver longitude—secondary	Subobserver east longitude of the secondary target
SSSOLLAT = "−1.07"/[deg] subsolar latitude—secondary	Subsolar latitude of the secondary target
SSSOLON = "190.18"/[deg] subsolar longitude—secondary	Subsolar east longitude of the secondary target

Note. The left column values are examples of what is expected in a real LICIACube data product.

<div align="center">**Table 2**</div>
<div align="center">FITS Metadata for the LUKE Raw Images</div>

Keyword and example	Description
SIMPLE = T/file conforms to FITS standard	Required in FITS standard
BITPIX = 8/number of bits per data pixel	LUKE raw images delivered to the SOC will always be 8 bit. Calibrated images are the result of applying the calibration files, themselves in 32 bit floating point, to the raw images. All are stored in big endian as per the FITS standard.
NAXIS = 2/number of data axes	Number of data axes; all LUKE raw images have two axes
NAXIS1 = 2048/length of data axis 1	Number of rows
NAXIS2 = 1088/length of data axis 2	Number of columns
EXTEND = T/FITS data set may contain extensions	By default, set to T so that we can add extensions if needed
DATE = "2018-08-25T09:23:89"/FITS header creation date YYYY-MM-DDTHH:MM:SS	Time fits file was created by the SOC. For calibrated and derived, it is the creation time of the product.
MISSION = "DART"/mission: DART	Name of mission
HOSTNAME = "LICIACube"/spacecraft name	LUKE is on the spacecraft named LICIACube
INSTRUME = "LUKE"/instrument name	Instrument name
APID	Application ID of science image data: the images themselves
TARGET = "DIDYMOS"/target object	Primary target object
MPHASE = "TERMINAL"/phase of the mission	The DART mission is divided into phases; this keyword states the phase during which the image was acquired.
IMG_TIME = "298271898.012320"/[s] image TOV	Start of image capture time in spacecraft clock notation. The number preceding the decimal point is integer seconds. The number after the decimal point is subsecond clock ticks, where each tick represents TBD microseconds.
IMG_UTC = "2022 OCT 01 10:28:09.600"/image TOV in UTC	Start of image capture time in UTC
SCLKNAME = "liciacube_sclk_0000.tsc"/SCLK file used for IMG_UTC	Name of SCLK file used to compute IMG_UTC
READOUT = "87.46666"/readout time in microseconds per line	Global readout time
EXPTIME = "0.156789"/[s] exposure time	Image exposure time in seconds
GAIN = 1 /gain setting	Detector gain setting
BINNING = "ON"/binning status	If binning is on or not
WINXSTA = "0"/X origin of window	Column where window starts. Window coordinates are with respect to a 1088 × 2048 image. The upper left-hand corner of the image plus header row is coordinate 0, 0. −1 if second windowing not applied.
WINYSTA = "0"/Y origin of window	Row where window starts. Window coordinates are with respect to a 1088 × 2048 image. The upper left-hand corner of the image plus header row is coordinate 0, 0. −1 if second windowing not applied.
WINXEND = "2048"/X end of window	Column where window ends. Window coordinates are with respect to a 1088 × 2048 image. The upper left-hand corner of the image plus header row is coordinate 0, 0. −1 if second windowing not applied.

Table 2
(Continued)

Keyword and example	Description
WINYEND = "2048"/*X* end of window	Row where window ends. Window coordinates are with respect to a 1088×2048 image. The upper left-hand corner of the image plus header row is coordinate 0, 0. −1 if second windowing not applied.
TRUNC = "MSB"/truncation mode	Defines whether the data are truncated using MSB or LSB. When binning is enabled, the truncation mode is MSB. When binning is disabled, the truncation mode is LSB.
RCNTTHST = 1/thruster firing flag	Flag for whether thrusters were fired within one settling time before this image; 1 = true, 0 = false (TBR)
AOCWX = 0/[deg s^{-1}] rotation speed on *X*-axis	Rotation speed of LICIACube frame *X*-axis
AOCWY = 0/[deg s^{-1}] rotation speed on *Y*-axis	Rotation speed of LICIACube frame *Y*-axis
AOCWY = 0/[deg s^{-1}] rotation speed on *Z*-axis	Rotation speed of LICIACube frame *Z*-axis
DETTEMP = 18.333/[degC] detector temperature	Detector temperature
EPHMETA = "LCC210701-EMK-RN-L211124-V001.mk"/ephemeris meta-kernel to be used	Ephemeris metakernel to be used
ATTMETA = "LCC201228-AMK-RN-L221124-V001.mk"/attitude meta-kernel to be used	Attitude metakernel to be used
CORT_UTC	UTC time at mid-exposure time (=IMGTIME+0.5EXPTIME) used to define attitude and representative observing geometry
CORTJDAT	Julian Ephemeris Date based at mid-exposure (=IMGTIME+0.5EXPTIME) used to define attitude and representative observing geometry
SOCQUATA = "0.10808003767484" /SC quaternion in J2000 (q0) using A CORT_UTC	Spacecraft quaternion computed by the SOC using SPICE and CORT_UTC
SOCQUATX = "−0.674302095900066" /SC quaternion in J2000 (q1) using CORT_UTC	
SOCQUATY = "−0.32453616895850" /SC quaternion in J2000 (q2) using CORT_UTC	
SOCQUATZ = "0.65445524213556" /SC quaternion in J2000 (q3) using appropriate CORT_UTC time	
BORE_RA = "326.459994"/[deg] boresight R.A.	Boresight R.A.
BORE_DEC = "−38.093559"/[deg] boresight decl.	Boresight decl.
CELN_CLK = "28.16" /[deg] celestial north clock angle	Celestial north clock angle
ECLN_CLK = "49.30" /[deg] ecliptic north clock angle	Ecliptic north clock angle
SUN_CLK="318.40"/[deg] Sun clock angle	Sunward direction clock angle
PXARCS = "1.02"/[arcsec] pixel scale	Pixel scale in arcseconds
PXMRAD = "4.96"/[microradians] pixel scale	Instantaneous field of view of a pixel in microradians. If BINNING = ON, this value is reported for a 2×2 binned pixel.
PHDIST = "1.04"/[au] heliocentric distance—primary	Distance between the Sun and the primary target in au
PSCRNG = "4.2622E+02"/[km] spacecraft range—primary	Distance between the spacecraft and the primary target center in kilometers
PSPHASE = "55.98"/[deg] solar phase angle—primary	Angle between the sunward direction and the direction to the spacecraft as observed from the primary target
PSELON = "73.49"/[deg] solar elongation—primary	Angle between the sunward direction and the direction to the primary target as observed from the spacecraft
PPPCLK = "228.64"/[deg] positive pole clock angle—primary	Positive pole clock angle of the primary target
PSUBLAT = "38.04"/[deg] subobserver latitude—primary	Subobserver latitude of the primary target
PSUBLON = "146.65"/[deg] subobserver longitude—primary	Subobserver east longitude of the primary target

Table 2
(Continued)

Keyword and example	Description
PSSOLLAT = "−1.07"/[deg] subsolar latitude—primary	Subsolar latitude of the primary target
PSSOLLON = "190.18"/[deg] subsolar longitude—primary	Subsolar east longitude of the primary target
SHDIST = "1.04"/[au] heliocentric distance—secondary	Distance between the Sun and the secondary target in au
SSCRNG = "4.2623E+02"/[km] spacecraft range—secondary	Distance between the spacecraft and the secondary target center in kilometers
SSPHASE = "56.14"/[deg] solar phase angle—secondary	Angle between the sunward direction and the direction to the spacecraft as seen from the secondary target
SSELON = "73.59"/[deg] solar elongation—secondary	Angle between the sunward direction and the direction to the secondary target as observed from the spacecraft
SPPCLK = "228.64"/[deg] positive pole clock angle—secondary	Positive pole clock angle of the secondary target
SSUBLAT = "38.09"/[deg] subobserver latitude—secondary	Subobserver latitude of the secondary target
SSUBLON = "146.46"/[deg] subobserver longitude—secondary	Subobserver east longitude of the secondary target
SSSOLLAT = "−1.07"/[deg] subsolar latitude—secondary	Subsolar latitude of the secondary target
SSSOLON = "190.18"/[deg] subsolar longitude—secondary	Subsolar east longitude of the secondary target

Note. The left column values are examples of what is expected in a real LICIACube data product.

Table 3
Additional FITS Metadata for the LEIA Calibrated Images

Keyword and Example	Description
BITPIX = 32/number of bits per data pixel	LEIA raw images delivered to the SOC will always be 16 bit. Calibrated images are the result of applying the calibration files, themselves in 32 bit floating point, to the raw images. All are stored in big endian as per the FITS standard.
RADCONV = 1.0/radiance conversion factor	Radiance conversion factor
CALFILE = "liciacube_leia_cal_001.fits"/ref calibration file	Name of calibration file used
BADMASKV = "−1E30"/value assigned to bad pixels	Pixel value assigned to bad pixels by the SOC
MISPXVAL = "1E32"/value assigned to missing pixels	Keyword created by MOC; value updated by pipeline
SATPXVAL = "1E30"/value assigned to saturated pixels	Pixel value assigned to saturated pixels by the SOC

Note. The left column values are examples of what is expected in a real LICIACube data product.

2. Plane 1: bad pixel map conventional value for the bad pixels.
3. Plane 2: dark rate in DN/s.
4. Plane 3: coeff x0 of the x0+x1*DN+x2*DN ∧ 2+x3*DN ∧ 3 radiometric conversion polynomial for corresponding (i, j) pixel.
5. Plane 4: coeff x1 of the x0+x1*DN+x2*DN ∧ 2+x3*DN ∧ 3 radiometric conversion polynomial for corresponding (i, j) pixel.
6. Plane 5: coeff x2 of the x0+x1*DN+x2*DN ∧ 2+x3*DN ∧ 3 radiometric conversion polynomial for corresponding (i, j) pixel.
7. Plane 6: coeff x3 of the x0+x1*DN+x2*DN ∧ 2+x3*DN ∧ 3 radiometric conversion polynomial for corresponding (i, j) pixel.

These files will be used according to what is depicted in Figure 3, as follows:

1. The bad pixels are identified, subtracted, and averaged.
2. The bias is subtracted.
3. The dark current is subtracted by taking into consideration the integration time and detector temperature.
4. Using the x0+x1*DN+x2*DN ∧ 2+x3*DN ∧ 3 radiometric conversion formula with the values of the coefficients stored in planes 3, 4, 5, and 6, the data are converted from DN to calibrated radiance.

The final calibration procedure will be accurately described by V. Della Corte et al. (2022, in preparation).

Data products resulting from the complete image processing (i.e., both raw and calibrated) are finally archived in a predefined directory structure able to ease the search and retrieval operations and ready to be used for the public Planetary Data System release after the LICIACube end of the mission (i.e., roughly 9 months after the DART impact).

Table 4
Additional FITS Metadata for the LUKE Calibrated Images

Keyword and Example	Description
BITPIX = 32/number of bits per data pixel	LUKE raw images delivered to the SOC will always be 8 bit. Calibrated images are the result of applying the calibration files, themselves in 32 bit floating point, to the raw images. All are stored in big endian as per the FITS standard.
RADCONV = 1.0/radiance conversion factor	Radiance conversion factor
NAXIS = 3/number of data axes	Number of data axes; all LUKE calibrated images have three axes
NAXIS3 = 3/length of data axis 3	Number of bands; all LUKE calibrated images have three bands
CALFILE = "LICIACube_LUKE_CAL_001.fits"/ref calibration file	Name of calibration file used
PLANE1 = "RED"/color of image plane	Color of image plane
PLANE2 = "GREEN"/color of image plane	Color of image plane
PLANE3 = "BLUE"/color of image plane	Color of image plane
BADMASKV = "−1E30"/value assigned to bad pixels	Pixel value assigned to bad pixels by the SOC
MISPXVAL = "1E32"/value assigned to missing pixels	Keyword created by MOC; value updated by pipeline
SATPXVAL = "1E30"/value assigned to saturated pixels	Pixel value assigned to saturated pixels by the SOC

Note. The left column values are examples of what is expected in a real LICIACube data product.

In particular, the directory structure will follow an "instrument, calibration level, mission phase" priority, as described here:

1. leia_raw
   (a) prelaunch
   (b) approach
   (c) terminal
   (d) post-impact
2. leia_calibrated
   (a) prelaunch
   (b) approach
   (c) terminal
   (d) post-impact
3. luke_raw
   (a) prelaunch
   (b) approach
   (c) terminal
   (d) post-impact
4. luke_calibrated
   (a) prelaunch
   (b) approach
   (c) terminal
   (d) post-impact.

The entire abovementioned process will be made automatic through a series of ad hoc developed Python packages. Once a new raw-from-telemetry image is made available on the MCC Secure File Transfer Protocol server, together with its metadata, the pipeline will start by downloading the files needed to generate the raw FITS file.

In order to be compliant with the PDS4 standard, each image needs to be accompanied by an XML label. Hence, the mentioned pipeline will also generate the accompanying PDS4 label, using some of the metadata already present in the FITS header.

The generation of the raw FITS from the raw-from-telemetry image can be considered almost instantaneous; therefore, the automatic process will finally load the data product in the correct directory. Afterward, the DART/LICIACube team can begin the download.

A similar pipeline has to be used for the calibrated FITS files, with the difference being that the input file, in this case, is not the raw-from-telemetry one but the raw FITS generated by the SOC pipeline, together with the required calibration file. As for the raw FITS files, an XML label (PDS4 compliant) will be generated and loaded in the expected directory to start the sharing with the DART/LICIACube team.

Another task pursued by the SOC is the generation of simulated images relative to the predicted LICIACube close approach with Dimorphos (see Pajola et al. 2022, this focus issue). These images have been generated based on the SSDC expertise in 3D planetary data visualization, the heritage of the MATISSE development, using the predicted spacecraft trajectories and instrument observation geometries defined in the SPICE kernels made available by the LICIACube navigation and instrument teams (Figure 4).

Starting from a preliminary set of trajectories, they would be precious for the modifications to the MATISSE tool needed for the LICIACube mission, described in the following section.

Since the shapes of the two asteroids to be imaged are not yet well constrained, we used adequately rescaled shape models for Ryugu (Watanabe et al. 2019) and Eros (Gaskell 2008) to make reasonable assumptions on the expected Didymos and Dimorphos shape and simulate it.

4. MATISSE Tool and Its Planned Development for LICIACube

MATISSE version 2.0 is presently available with a totally new appearance and brand-new capabilities, making it a real hub for the planetary sciences community (see Figure 5).

Among these new functionalities, it is worth mentioning the use of a database management system (DBMS) best suited for geospatial analysis, such as PostgreSQL with its plug-in PostGIS, thus allowing one to correctly manage complex data
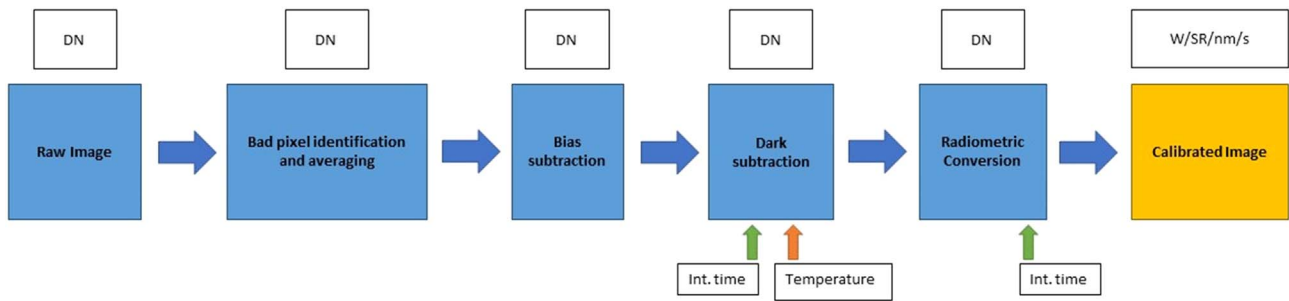
Figure 3. Design of the calibration pipeline.
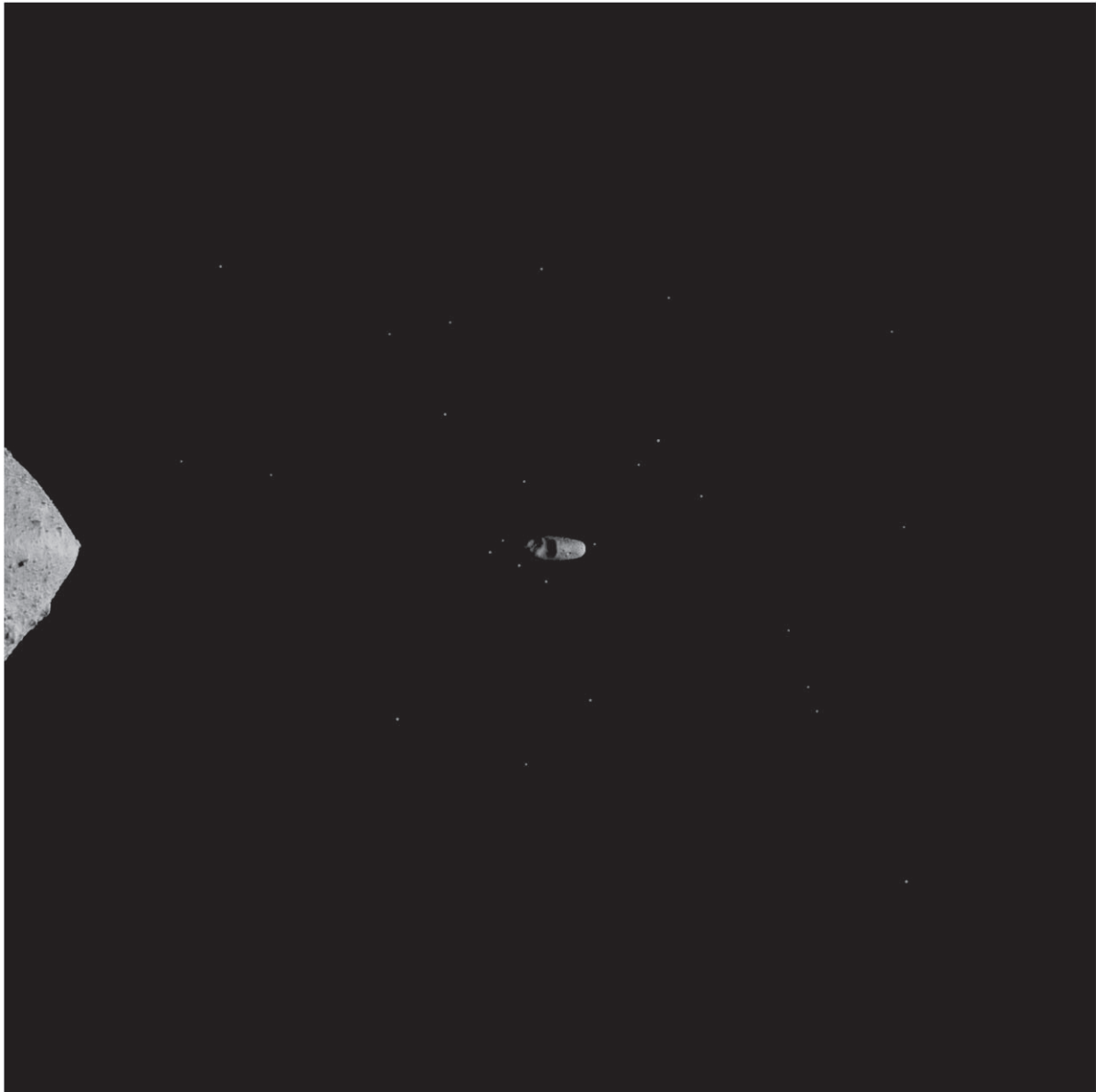
Figure 4. LEIA simulated image with spatial resolution corresponding to that expected at LICIACube closest approach.

sets mapping rocky surfaces from different targets in the solar system, thanks to a series of customized tables.

Exploiting this architecture, each mission, instrument, and target has its own identification tag (ID), so that a unique combination of these three IDs identifies the data set to be searched.

This last ID is used to link the metadata table (in which parameters such as acquisition time, shape of the field of view, spatial coordinates of the observations and emission, and incidence and phase angles are stored) to the corresponding data set.
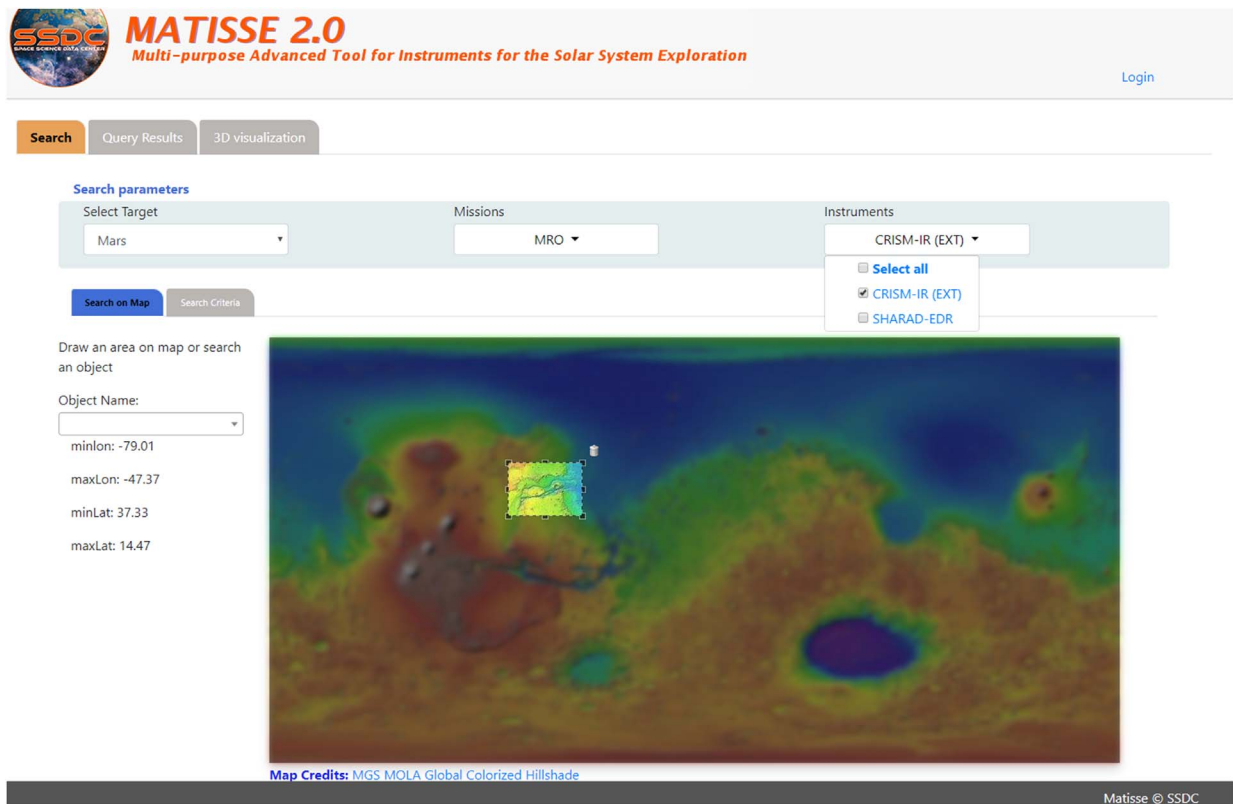
Figure 5. The MATISSE 2.0 homepage, with the map for selecting data.
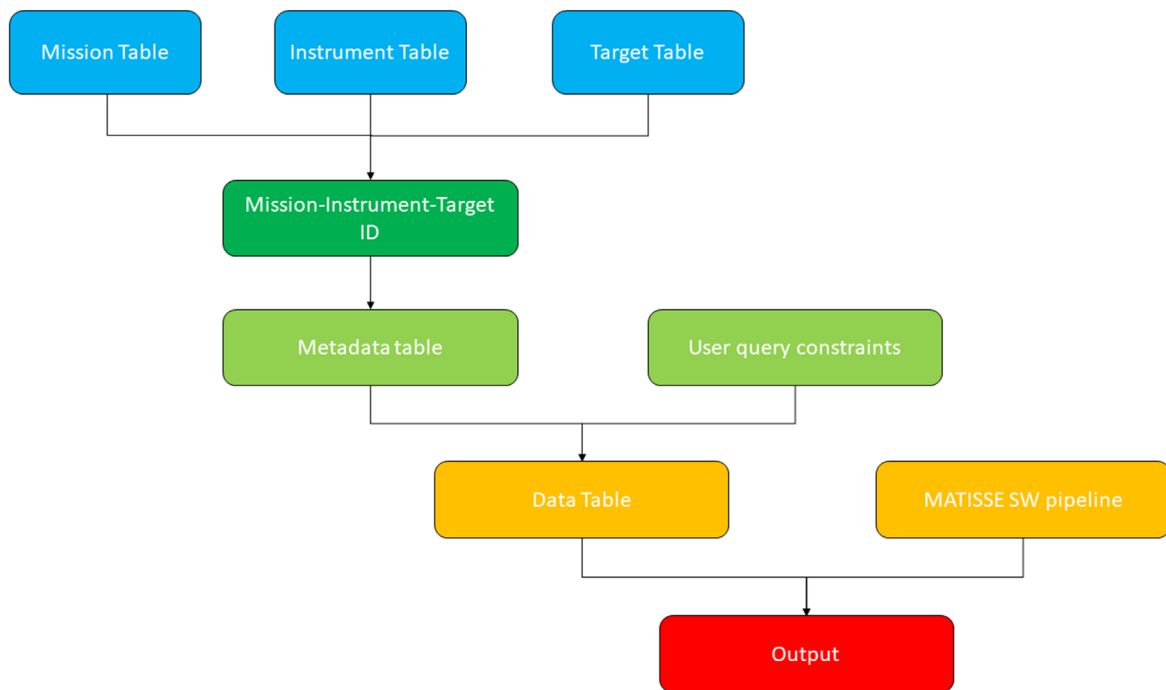

Figure 6. Schematic representation of the steps used by MATISSE to search and process data.

Therefore, it is possible to search for data using temporal, spatial, and geometrical constraints; the query is performed matching the user-inserted constraints with the values found in the metadata table, and, after the query returns results, the user can choose the data to be processed. These are stored in another table, linked to the metadata table thanks to its ID, thus allowing one to find and process the data belonging to the selection (see Figure 6 for a schematic representation of the steps used by MATISSE to search and process data).

Since this tool is particularly useful for data acquired over the irregular surfaces typical of small bodies, it is straightforward thinking to add LICIACube data to its database.
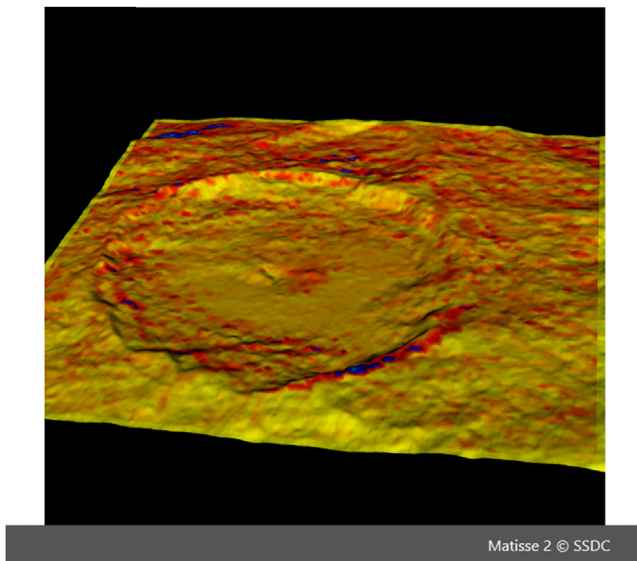
Figure 7. Surface temperature over the dwarf planet Ceres, as computed by the thermophysical model made available by MATISSE 2.0.

Therefore, within MATISSE, it would be possible to explore LEIA and LUKE observations in an optimal way by using both its data search and 3D data projection capabilities.

As the LICIACube data set will be processed and stored on SSDC local machines as a PDS4 bundle, together with ancillary data products useful for computation of observation geometries, its ingestion by MATISSE would be fairly easy.

In addition, a series of new functionalities recently added or under development and that will be accurately described in the following could further enhance the MATISSE data analysis capabilities for LICIACube. Among these, there are the airless body thermophysical model by Rognini et al. (2020; see Figure 7) and the data selection based on surface character-istics, such as geological units (Camplone et al. 2021; see Figure 8).

The airless body thermophysical model is already available in MATISSE, giving as output surface temperatures for Ceres and Mercury, after the user set up the type of surface (between Moondust 1, Moondust 2, Dust, Fine regolith, Regolith, Coarse sand and Bedrock; see Rognini et al. 2020 for further details on these surface types) and the start and stop computing times (being careful to make the model run for a sufficiently long period in order to allow its differentiation from initial conditions).

This model is now under refinement, allowing one to compute reliable outputs not only for larger bodies (i.e., dwarf planets and planets) but also for the smallest objects present in the solar system, with the characteristic rubble-pile structure, as Didymos and maybe Dimorphos are expected to be. When the final version of the model will be ready for use in MATISSE, it will be used to compare LICIACube observations with modeled predictions, so that a new, in-depth analysis of the data could be performed.

The geological unit selection option is a brand-new MATISSE feature, likely to be released, at least in a beta version, through 2022 and will be extremely useful to pave the way for using MATISSE as an advanced GIS-like tool.

In order to do this, a series of geometries representing the projections over the different celestial bodies of geological units of interest are currently being selected and imported into the MATISSE database.

After the completion of this phase, the user could perform queries to the data, using as input not only classical spatial constraints but also geometries from published geological maps (e.g., Pondrelli et al. 2011; Williams et al. 2019; Wright et al. 2019) with semantic meaning. In this way, the user would be allowed to search for observational data acquired over areas with the same geological history, so that a comparative analysis could be easily conducted.

These two functionalities would be better exploited if accompanied by a series of new features we are planning to add and test with the LICIACube data. As an example, it would be extremely useful for the team, and for the planetary community in general, to select, by hand or using artificial intelligence algorithms, particular areas of the observation, such as visible boulders or fractures, in an interactive way so that a targeted analysis could be easily performed.

These further developments have not started yet, but we are planning, in collaboration with the scientific team, to make some of them available for the LICIACube data after their science mission phase, so that they can be used by the team when the data set is progressively downlinked in the months following the observations.

5. Expected Impact of SSDC Activities on the LICIACube Mission

As demonstrated by previous works, the possibility of accessing planetary data through an interactive web-based platform built on a DBMS designed for geospatial applications, using standard formats for data and metadata able to make them as compliant as possible with the FAIR (findable, accessible, interoperable, and reusable; Collins et al. 2018) principles and with the addition of interactive 2D/3D outputs, facilitates the process of gathering useful information from the acquired data, thus improving the scientific production.

This is exactly what MATISSE is thought to allow, and, for the LICIACube mission in particular, the fact that the data management and processing activities are performed on SSDC servers and under SSDC responsibility greatly encourages the applications to this tool.

As soon as the observation geometries are computed, LEIA and LUKE images will be loaded on the MATISSE database, together with their relevant metadata, so that team members can look for specific observations and analyze them in the advanced ways MATISSE already allows.

Since the data downlink will last for several months, the public release of data to the Planetary Data System is planned for 9 months after the closest approach. At that point, all of the data collected will also be made available to the public by means of MATISSE.

In addition, when the dedicated developments are ready, even more complex analysis could be performed directly on the web, speeding up the analysis process.

The user would be able to compare observed areas looking for surface features, such as boulders, or compare observational data with modeled ones.

Figure 8. Martian CTX data selected by means of MATISSE 2.0 using the geological units. The image represents Firsoff Crater with data from the "Aeolian/mass wasting/impact craters" geological unit, as described by Pondrelli et al. (2011).

ORCID iDs

Angelo Zinzi ⓘ https://orcid.org/0000-0001-5263-5348
Stavro L. Ivanovski ⓘ https://orcid.org/0000-0002-8068-7695
Maurizio Pajola ⓘ https://orcid.org/0000-0002-3144-1277
Alessandro Rossi ⓘ https://orcid.org/0000-0001-9311-2869
Olivier Barnouin ⓘ https://orcid.org/0000-0002-3578-7750
John R. Brucato ⓘ https://orcid.org/0000-0002-4738-5521
Gabriele Cremonese ⓘ https://orcid.org/0000-0001-9021-1140
Massimo Dall'Ora ⓘ https://orcid.org/0000-0001-8209-0449
Simone Ieva ⓘ https://orcid.org/0000-0001-8694-9038
Davide Perna ⓘ https://orcid.org/0000-0002-4545-3850
Giovanni Poggiali ⓘ https://orcid.org/0000-0002-3239-1697
Pasquale Palumbo ⓘ https://orcid.org/0000-0003-2323-9228

References

Camplone, V., Zinzi, A., Massironi, M., et al. 2021, Europlanet Science Congress, 15, EPSC2021–489
Cheng, A. F., Rivkin, A. S., Michel, P., et al. 2018, P&SS, 157, 104
Ciarniello, M., Raponi, A., Capaccioni, F., et al. 2016, MNRAS, 462, S443
Collins, S., Genova, F., Harrower, N., et al. 2018, Turning FAIR into reality: final report and action plan from the European Commission expert group on FAIR, data Publications Office, 2018, https://data.europa.eu/doi/10.2777/54599
Dotto, E., Banaszkiewicz, M., Banchi, S., et al. 2021, LPSC, 52, 1971
Dotto, E., Della Corte, V., Amoroso, M., et al. 2021, P&SS, 199, 105185
Gaskell, R. W. 2008, Gaskell Eros Shape Model Bundle V1.1, urn:nasa:pds:gaskell.ast-eros.shape-model::1.1, NASA, Planetary Data System, doi:10.26033/d0gq-9427
Longobardo, A., Palomba, E., Capaccioni, F., et al. 2017, MNRAS, 469, S346
Longobardo, A., Zinzi, A., Capria, M. T., et al. 2018, AdSpR, 62, 2317
Pajola, M., Barnouin, O., Lucchetti, A., et al. 2022, PSJ, submitted
Poggiali, G., Brucato, J. B., Hasselmann, P. H., et al. 2022, PSJ, submitted
Pondrelli, M., Rossi, A. P., Ori, G. G., et al. 2011, E&PSL, 304, 511
Quirico, E., Moroz, L. V., Schmitt, B., et al. 2016, Icar, 272, 32
Rognini, E., Capria, M. T., Tosi, F., et al. 2020, JGRE, 125, e05733
Tosi, F., Capaccioni, F., Capria, M. T., et al. 2019, NatAs, 3, 649
Watanabe, S., Hirabashi, M., Hirata, N., et al. 2019, Sci, 364, 268
Williams, D. A., Buczkowski, D. L., Crown, D. A., et al. 2019, LPI Contribution, 2066, 7001
Wright, J., Rothery, D. A., Balme, M., et al. 2019, Journal of Maps, 15, 2
Zinzi, A., Camplone, V., Rognini, E., et al. 2021, LPI Contribution, 2549, 7018
Zinzi, A., Capria, M. T., Palomba, E., et al. 2016, A&C, 15, 16
Zinzi, A., Ciarniello, M., Della Corte, V., et al. 2018, AdSpR, 62, 2306
Zinzi, A., Giardino, M., Giunta, A., et al. 2021, LPI Contribution, 2549, 7032